Quarterly Progress Report

N01-NS-1-2333

Restoration of Hand and Arm Function by Functional Neuromuscular Stimulation

Period covered: October 1, 2004 to December 31, 2004

Principal Investigator: Robert F. Kirsch, Ph.D.

Co-Investigators:

Patrick E. Crago, Ph.D.
P. Hunter Peckham, Ph.D.
Warren M. Grill, Ph.D.
J. Thomas Mortimer, Ph.D.
Kevin L. Kilgore, Ph.D.
Michael W. Keith, M.D.
David L. Wilson, Ph.D.
Dawn Taylor, Ph.D.
Joseph M. Mansour, Ph.D.
Jeffrey L. Duerk, Ph.D.
Wyatt S. Newman, Ph.D.
Harry Hoyen, M.D.
John Chae, M.D.
Jonathon S. Lewin, M.D.
Dustin Tyler, Ph.D.

Program Manager: William D. Memberg, M.S.

Case Western Reserve University
Wickenden 407
10900 Euclid Avenue
Cleveland, OH 44106-7207
216-368-3158 (voice)
216-368-4969 (FAX)
rfk3@po.cwru.edu

Contract abstract

The overall goal of this contract is to provide virtually all individuals with a cervical level spinal cord injury, regardless of injury level and extent, with the opportunity to gain additional useful function through the use of FNS and complementary surgical techniques. Specifically, we will expand our applications to include individuals with high tetraplegia (C1-C4), low tetraplegia (C7), and incomplete injuries. We will also extend and enhance the performance provided to the existing C5-C6 group by using improved electrode technology for some muscles and by combining several upper extremity functions into a single neuroprosthesis. The new technologies that we will develop and implement in this proposal are: the use of nerve cuffs for complete activation in high tetraplegia, the use of current steering in nerve cuffs, imaging-based assessment of maximum muscle forces, denervation, and volume activated by electrodes, multiple degree-of-freedom control, the use of dual implants, new neurotization surgeries for the reversal of denervation, new muscle transfer surgeries for high tetraplegia, and an improved forward dynamic model of the shoulder and elbow. During this contract period, all proposed neuroprostheses will come to fruition as clinically deployed and fully evaluated demonstrations.

Summary of activities during this reporting period

The following activities are described in this report:

- *Predicting reach goal in a continuous workspace for command of a brain-controlled upper-limb neuroprosthesis*
- *Wireless data acquisition module for use with a neuroprosthesis*
- *Neural network controller for an upper extremity neuroprosthesis*
- *Feed-forward control of neuroprosthetic systems characterized by redundant muscles acting on multiple degrees of freedom*
- *An implanted neuroprosthesis for electrical stimulation through nerve- and muscle-based electrodes and myoelectric recording*

Predicting reach goal in a continuous workspace for command of a brain-controlled upper-limb neuroprosthesis

***Contract section**:* E.1.a.iv Command sources for high tetraplegia

Abstract

A controller for an upper-limb functional electrical stimulation system could use an intended reach *goal* to generate a set of stimulation patterns that would move the hand to the desired location via a reasonably naturalistic velocity profile. Although discrete classifiers have been successfully used to predict a movement goal from a fixed number of possible reach locations using neural activity recorded during movement planning, practical implementation of this paradigm for use in upper-limb neuroprostheses requires the ability to predict a reach goal anywhere within a person's workspace. Using neural data collected from monkeys during brain-controlled movements of a virtual cursor and robotic arm, we evaluated how well the direction versus magnitude of the final movement goal could be predicted from varying lengths of neural

data collected after the target appeared. Although a majority of the channels were significantly modulated with intended movement direction, only 10-20% showed any significant modulation related to the magnitude of the movement goal. We propose a method of trajectory generation that could use the more reliably encoded directional information in the neural activity to control both magnitude and direction of a goal oriented reaching movement.

Introduction

Recently, many studies have decoded intended movement from various parts of a monkey's cortex and used that prediction to move a computer cursor or robotic device in real time [1-7]. This type of a movement-related brain-machine interface (BMI) has many potential applications for severely paralyzed individuals. We are particularly interested in using brain recording technologies as a command source for restoring arm and hand function in people with spinal cord injures at the C4 level or higher. Our colleagues in the Cleveland Functional Electrical Stimulation (FES) Center are expanding the current stimulation technology to be able to restore all the degrees of freedom necessary to regain practical movements in a paralyzed arm and hand [8-10]. However, command signal options to direct FES-generated limb movements are limited to what these severely paralyzed individuals can produce from the neck up. This includes facial movements, eye gaze direction, head tilt, voice commands, sip n' puff, tongue-touch keypads, etc. Although these options may be effective, they are cumbersome and can interfere with eating, talking, and normal social interactions. A more natural option would be to access intended arm and hand movements directly from the brain.

Previously, we have shown that monkeys can learn to make long continuous sequences of target-directed movements of a brain-controlled virtual cursor or robotic arm in three dimensions using unit activity from the arm area of the motor and premotor cortices [1, 2]. In that study, the animals had continuous proportional control of the X, Y, and Z trajectory components throughout the movement. Continuous proportional control of one's limb in space is necessary for many activities of daily living such as drawing, combing one's hair, and shaving. However, many practical activities consist primarily of reach-to-grasp movements. Several studies have recently demonstrated that the goal of an intended reach can often be predicted from the neural activity detected during the planning phase of the reaching movement [5-7]. The potential benefit of decoding the intended reach goal instead of decoding continuous path details is that the controller of an upper-limb FES system could execute the movement on its own once the reach goal is known. This could reduce the level of mental effort required of the user, and the FES controller could be programmed to make relatively straight trajectories with bell-shaped velocity profiles to produce more naturalistic movement paths than what may be produced when continuous brain control is used throughout the movement.

Studies that have focused on goal prediction have used discrete classifiers to predict which of a fixed number of targets an animal was planning on moving to. This process of discrete target selection is particularly well suited to certain computer-based selection tasks where the desired letters or icons can be displayed within the limited number of discrete locations that the neural classifier can accurately identify. However, this type of system is less practical for goal-directed reaches in the physical world where the objects can be located in a continuum of positions throughout the workspace.

Methods

The details of the experimental setup have been reported elsewhere [1, 2] and are summarized here. A Rhesus macaque was trained to do a three-dimensional (3D) center-out arm movement task viewed in a virtual environment. The animal was rewarded for moving his arm, and thus the virtual cursor, from the center of the workspace to one of eight outer targets that would appear in his virtual environment. Once trained in the center-out task, the animal was implanted with microwire electrode arrays in the arm area of the motor and premotor cortices. The animal then had to do the same 3D virtual center-out task by moving the virtual cursor directly with its recorded neural activity while both of its arms were restrained.

The decoding algorithm used to convert neural firing rates into cursor movements was iteratively determined through a coadaptive training process. At each time step, change in cursor position was determined by a linear sum of each unit's normalized firing rate times a set of X, Y, and Z coefficients. These coefficients were iteratively refined during each training session based on the neural activity produced by the animal as it attempted to move the brain-controlled cursor. In this parallel learning process, the animal adapted its neural output to be more effective in moving the virtual cursor via the current decoder. Simultaneously, the decoder was regularly adapted to be more effective based on the neural activity that the animal had produced in recent trials. This parallel learning environment allowed the animal to explore new, more-effective ways of encoding intended movement because the decoding algorithm could track and adjust to learning-induced changes in the animals firing patterns.

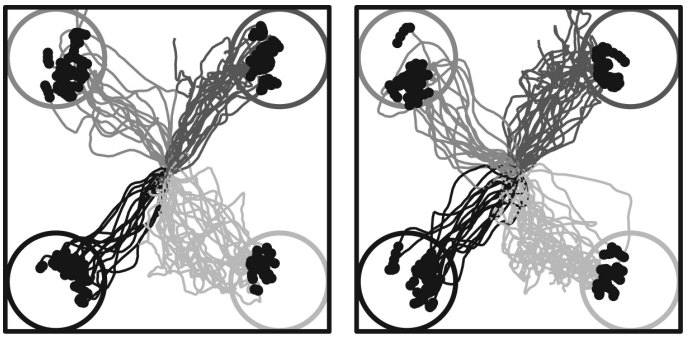

Figure 1. Center-out brain-controlled cursor trajectories to eight radial targets located at the corners of an imaginary cube. The eight sets of 3D trajectories are split into two plots for easier 2D viewing. Trajectory shading is color-coded to match the intended target (shaded outer rings). Black dots indicate when the target was successfully hit.

On some days, a six-degree-of-freedom robotic arm was inserted into the control loop. The monkey still viewed the 3D center-out task in the virtual environment. However, instead of controlling the cursor directly with its decoded brain signals, the brain signals controlled the movements of the robot, and a position sensor on the end of the robot controlled the location of the cursor in the virtual workspace.

Once the coadaptive process had converged to a stable set of coefficients, the coefficients were held constant and the animal had to move the robot to targets that appeared at random locations distributed throughout the virtual workspace at radial distances varying from 3-9 cm.

Both the average firing rates and linear filters were used to predict intended movement *magnitude* (i.e. distance between start position and target) using the firing activity of each unit immediately after the target appeared. Data segments tested varied from 90-660 msec. Each unit's initial firing rate was also tested, via linear regression, for significant modulation with respect to movement *direction* (unit vector pointing from the start position to the target) and to the *total movement* (full vector between the start position and the target).

The 400 movement trials were also randomly assigned to ten different training and testing sets. Units in the training set that were significantly modulated with desired movement

magnitude within a 75% level of confidence where then used to predict movement magnitudes on the testing data via linear filters.

Results

The coadaptive training process regularly converged on a decoding algorithm that enabled the animal to fairly accurately move the brain-controlled cursor to the targets. An example of brain-controlled trajectories to the eight targets is shown in Figure 1. More details of the general results of this coadaptive training have been published elsewhere [1, 2].

Figure 2 plots the percentage of units whose average firing rates were significantly modulated (alpha=0.05) with magnitude, direction, or total movement (incorporates both magnitude and direction). While most units where significantly modulated with movement direction or total movement, only a small percentage showed modulation with movement magnitude.

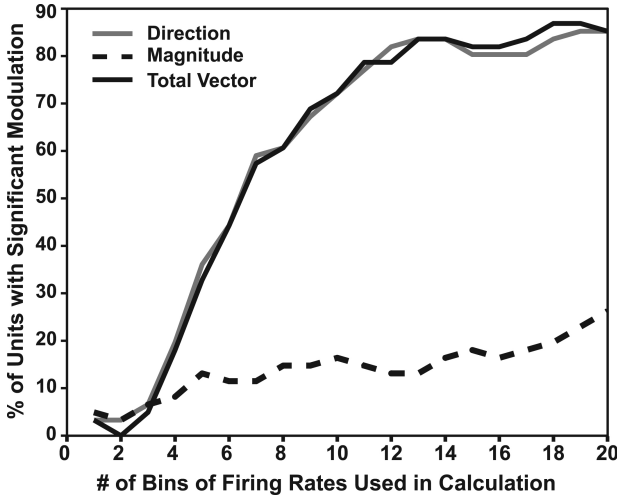

Figure 2. Percentage of recorded units whose firing rates were significantly modulated with movement direction, movement magnitude, and total movement vector from start position to target. Significance modulation was determined by linear regression (alpha=0.05) using firing rates averaged over different numbers of bins. Rates used in the brain control task were binned into 90 msec moving averages and updated every 30 msec. These bins of firing rates were further combined and averaged here. Therefore, one bin contains 90 msec of data, two bins encompass 120 msec of data, three bins encompass 150 msec of data, etc. with firing rates at the outer edges of the spread weighted less because they are not contained in overlapping bins.

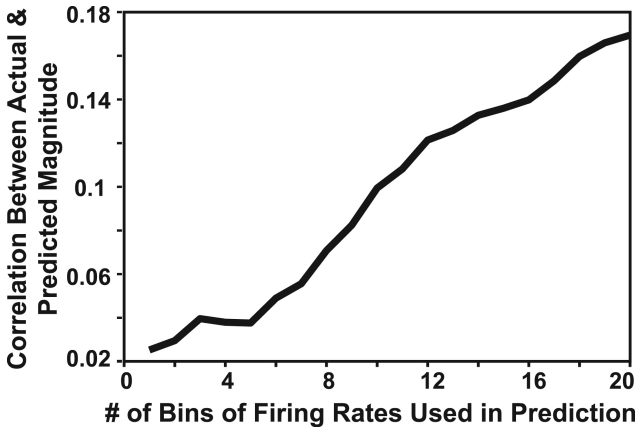

Figure 3. Average correlation coefficients for predicted versus actual movement magnitudes from the ten different combinations of training/testing data.

When predicting movement magnitude in the testing sets using linear filters generated from the training data, the correlation between actual and predicted movement magnitude was always positive for filter lengths of five bins or more. However, average correlation coefficients were still very low, even at longer filter length as shown in Figure 3.

Discussion

Based on these offline prediction results and the small percentage of units that showed any significant modulation with movement magnitude, accurate prediction of the intended magnitude of a reach goal from a continuum of possible magnitudes is unlikely in a brain-controlled upper-limb FES system. However, movement direction can be decoded fairly

accurately from the initial movement attempt as previously reported and as illustrated by the fairly reasonable directional accuracy throughout the trajectories in Figure 1. Directional accuracy greatly improved with use of adaptive decoding algorithms and regular practice. It may be that subjects will learn to also encode reach magnitude more accurately with regular practice if their limb controller utilizes that information in trajectory planning.

Even if reach magnitude prediction from the initial neural activity doesn't improve with practice, including an online correction factor may still enable accurate goal-oriented trajectory production. The controller would initiate a movement with an appropriate bell-shaped velocity profile using its best estimate of the intended magnitude and direction. Because trajectories will be programmed to have different bell-shaped velocity profiles for different reach magnitudes, the user should be able to anticipate what the final reach position will be from this trajectory (much like a baseball player can learn to anticipate where a ball will land based on the evolving trajectory). The limb controller will scale the velocity profile up or down in both time and peak velocity based on desired reach magnitude. Therefore, larger reach distances will have a longer initial acceleration time, a higher initial acceleration, and a higher, later peak velocity compared to shorter reach distances. These clues early on in the movement may enable the user to predict eventual reach distance and create a neural 'error signal' that can be used to correct the evolving trajectory en route.

Because reach magnitude errors result in either overshooting or undershooting the target distance, the movement vector needed to correct for these two conditions have opposite directions and are therefore easily conveyed by the subject's neural activity. The subject would either think move toward the target or move away from the target depending on if the subject anticipated an under or overshoot of the reach goal respectively. These opposite directional signals would work like an accelerator or a brake on the evolving velocity profile. Although the *magnitude* of the 'acceleration' or 'braking' correction vector is unlikely to be well encoded in the neural signal, the size of its effect on the evolving trajectory can be adjusted based on the *duration* that the user makes the correction signal.

This form of initial reach goal estimation and en route trajectory correction should enable a neuroprosthesis controller to utilize the higher resolution directional information in the neural signal to make target-directed reaching movements within a continuum of possible locations. Using brain activity to form preprogrammed trajectories to reach goals with natural velocity profiles instead of having the limb under continuous brain control throughout the movement may result in smoother, more natural looking reaching movements. However, for this to be true, the subjects need to be able to anticipate the final reach position that will result from the current velocity profile and 'accelerate' or 'brake' for the appropriate duration to make any needed adjustments to the evolving trajectory.

End-point correction based on visual feedback is an integral part of normal arm movements. However, it is unknown how accurately subjects can predict final reach location from evolving trajectories and use the duration of a constant magnitude correction signal to correct for any perceived errors. It is likely that this will be possible with slower reaching movements but not rapid movements. We are currently designing a study to evaluate these issues of end-point prediction and correction in humans.

Acknowledgment

Data used in this analysis were collected at Arizona State University in the lab of Dr. Andrew Schwartz and funded by NIH contracts N01-NS-6-2347, and N01-NS-9-2321, and by a

Whitaker Foundation Fellowship. Current data analysis was done in Cleveland and funded by the Cleveland VA Medical Center, NIH contract N01-NS-1-2333, the Ron Shapiro Charitable Trust, NIH Medical Scientist Training Program Grant #T32GM07250, NIH Integrated Engineering and Rehabilitation Training Grant #9T32EB04314-06, and NIH NINDS fellowship F30-NS50913-01.

REFERENCES

[1] Taylor, D.M., S.I.H. Tillery, and A.B. Schwartz, "Direct cortical control of 3D neuroprosthetic devices," *Science*, vol. 296, pp. 1829-1832, 2002.
[2] Taylor, D.M., S.I.H. Tillery, and A.B. Schwartz, "Information conveyed through brain-control: cursor versus robot," *Neural Systems and Rehabilitation Engineering, IEEE Transactions on*, vol. 11, pp. 195-199, 2003.
[3] Serruya, M.D., et al.," Instant neural control of a movement signal," *Nature*, vol. 416, pp. 141-142, 2002.
[4] Carmena, J.M., et al., "Learning to control a brain-machine interface for reaching and grasping by primates," *Public Library of Science*, vol. 1, pp. 1-16, 2003.
[5] Musallam, S., et al., "Cognitive control signals for neural prosthetics," *Science*, vol. 305, pp. 258 – 262, 2004.
[6] Ryu, S.I., et al., "High speed neural prosthetic icon positioning," *Conference proceeding of the 34th annual Society for Neuroscience meeting*, San Diego, CA, Program # 263.1, 2004
[7] Santhanam, G., S.I. Ryu, and K.V. Shenoy, "High information transfer rates in a neural prosthetic system," *Conference proceeding of the 34th annual Society for Neuroscience meeting*, San Diego, CA, Program # 263.2, 2004
[8] Kirsch, R.F., et al., "Model-based development of neuroprostheses for restoring proximal arm function," *J Rehabilitation Research and Dev*, vol. 38, pp. 619-626, 2001.
[9] Peckham, P.H., et al., "An advanced neuroprosthesis for restoration of hand and upper arm control using an implantable controller," *J Hand Surg [Am],* vol. 27, pp. 265-276, 2002.
[10] Keith, M.W. and H. Hoyen, "Indications and future directions for upper limb neuroprostheses in tetraplegic patients: a review," *Hand Clin*, vol. 18, pp. 519-528, viii, 2002.

Wireless Data Acquisition Module for Use with a Neuroprosthesis

Contract section: E.1.a.v Sensory feedback of contact and grasp force

Abstract

A general wireless data acquisition module (WDAM) is being developed for use with a neuroprosthesis. The WDAM is intended to be used with sensors such as the shoulder or wrist position transducer, finger-mounted joysticks, or remote on-off switches. Currently these sensors are connected to a controller via cables, which are cosmetically unappealing to the user and often get caught on wheelchairs, causing them to be damaged. Switch-activated transmitters mounted on walkers have been used previously in FES applications [1]. Recent advances in wireless technology have reduced the complexity and size of the wireless circuitry and have increased the likelihood that a small, low power, reliable wireless link could be assembled from commercially available components.

Methods

In the current quarter, tests were performed to identify an inconsistent decrease in the transmission success that was seen in some of the orientation sensitivity measurements that were made in the previous quarter. The ability of a single 'master' module to communicate to multiple 'slave' modules was demonstrated. In addition, a secondary (rechargeable) battery was identified that had acceptable capacity and size for the WDAM applications. Longevity and performance tests were performed on this battery.

Orientation sensitivity variability

In the previous quarter's report (QPR#14, Jul-Sept 2004), measurements of the WDAM's transmission success at different distances and orientations showed an occasional drop in the transmission success rate from around 95% to around 80%. One of the potential causes was a battery-connector cable that was being used to make it easier to switch batteries. The cable was longer than it needed to be and could have picked up electrical noise. Tests were performed with a shorter, twisted-pair cable to see whether this eliminated the variability.

Multiple 'slave' demonstration

All of the tests presented in previous progress reports consisted of one WDAM communicating with another WDAM. The ability of a module to communicate with more than one module had not been presented. To demonstrate this capability, one WDAM was programmed to be a 'master' module, which can request data from one or more 'slave' modules. The 'master' module was first programmed to request data just from one of the 'slave' modules, then just from a second 'slave' module. Then the 'master' module was programmed to alternate its data requests (see Table 1). Tests were performed with the 'slave' modules turned on and off to demonstrate the effect on transmission success. A CRC error-checking algorithm was used to determine if the data was received properly. For each test, 1000 data requests were sent, and the number and types of errors were counted and reported to a PC via a serial connection.

RechargeableBattery

Although a small zinc-air coin cell battery has been identified for the WDAM that has acceptable longevity (65-75 hours of use), there was some concern about the practicality of having the user open the enclosure and change the battery every couple of weeks. To alleviate this concern, a secondary (rechargeable) battery has been identified that is an acceptable size and has sufficient capacity for the intended applications. The battery is a lithium

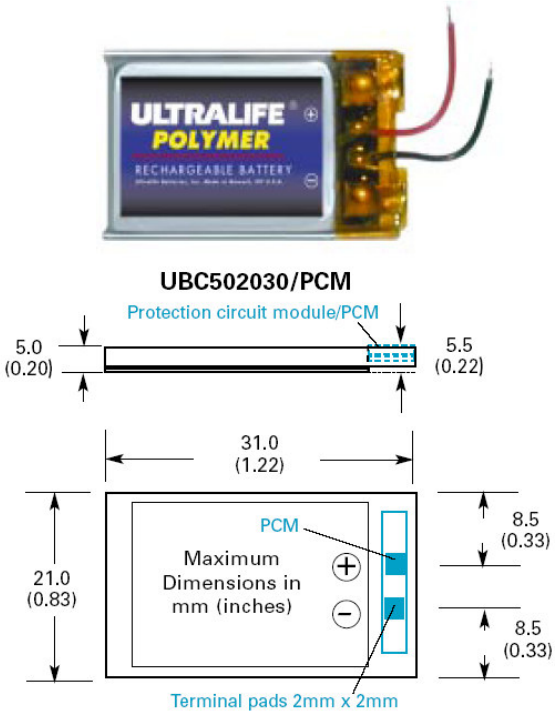

Figure 4. Rechargeable battery.

polymer rechargeable cell in a low-profile prismatic pack (see Figure 4). The size of the battery is 31 mm long, 21 mm wide and 5.5 mm high. This size fits well with the proposed dimensions of the miniaturized version of the WDAM, so that the battery can be placed underneath the circuitry. The battery has a nominal capacity of 180 mA·hr.

The actual capacity of this battery was evaluated in two ways. The first method was identical to the one used to evaluate other batteries for the WDAM. The battery was connected to a WDAM that was configured as a 'slave'. A 'master' WDAM continuously requested data from the 'slave'. The 'master' WDAM was serially connected to a PC, which recorded the status at 5 minute intervals. The capacity of the battery was determined by measuring the average current draw and identifying when the 'slave' module stopped transmitting data.

A second method that was used to evaluate the battery capacity was to use a commercially-available battery testing system (Arbin Instruments, College Station, TX). This system allows a programmable test protocol, where one can repeatedly charge and discharge a rechargeable battery at preset voltage and current levels, while these parameters are monitored and recorded.

Results

Orientation sensitivity variability

Observation of the transmitted data on an oscilloscope indicated that more electrical noise existed with the longer, untwisted battery cable than with a shorter, twisted-pair cable. When the original cable was placed in a position where the noise was maximized, and then was replaced with the twisted-pair cable, the transmission success rate improved from 78.5% to 96.0%. A repeat of the distance and orientation measurements with the new battery cable showed that the occasional drop in transmission success had been eliminated.

Multiple 'slave' demonstration

When the 'master' module was tested with each 'slave' module separately, the transmission success rate was around 96% (Table 1). When the 'master' module was programmed to alternate the data request between the 2 'slave' modules, the success rate was similar. To further demonstrate that the data was coming from both 'slave' modules, tests were performed with one of the 'slave' modules off. When this was done, the success rate was approximately half of the success rate with both 'slaves' on.

Test	% Acknowledged
Master to Slave1 only	95.3%
Master to Slave2 only	96.6%
Master alternating between slaves, Slave 1 **on**, Slave 2 **off**	49.3%
Master alternating between slaves, Slave 1 **off**, Slave 2 **on**	49.3%
Master alternating between slaves, Slave 1 **on**, Slave 2 **on**	95.4%

Table 1. Single 'master', multiple 'slave' test results.

RechargeableBattery

The voltage produced by the lithium polymer rechargeable battery was higher (4.09 V) than the primary batteries that had been tested previously (Table 2). This allowed the power regulator to draw less current (2.7 mA). The battery was able to power the module continually for over 68 hours, producing a measured capacity of 184 mA·hrs.

Table 2. Wireless Data Acquisition Module Battery Tests

Battery Type	Brand	Model	Size (Diam. x Ht.) (mm)	Rated Capacity (mA-hr)	Starting Voltage (V)	Ending Voltage (V)	Current Draw (mA)	Running Time (hrs)	Actual Capacity (mA-hrs)
Primary									
Zinc Air	Energizer	675	11.6 x 5.4	600	1.38	0.99	9.5	**64.9**	**617**
Lithium	Energizer	2032	20.0 x 3.2	225	3.2	0.9	3.0	**40.9**	**123**
Silver Oxide	Duracell	76S	11.6 x 5.3	175	1.6	0.1	6.3	**28.6**	**180**
Lithium	Duracell	1/3N	10.8 x 11.6	160	3.25	0.93	3.4	**32.9**	**112**
Lithium	Tadiran	TL5186	22.5 x 7.5	400	3.66	0.97	3.2	**40.8**	**131**
Rechargeable									
Lithium Polymer	Ultralife	UBC502030	21.0 x 31.0 x 5.5	180	4.09	0.00	2.7	**68.5**	**184**

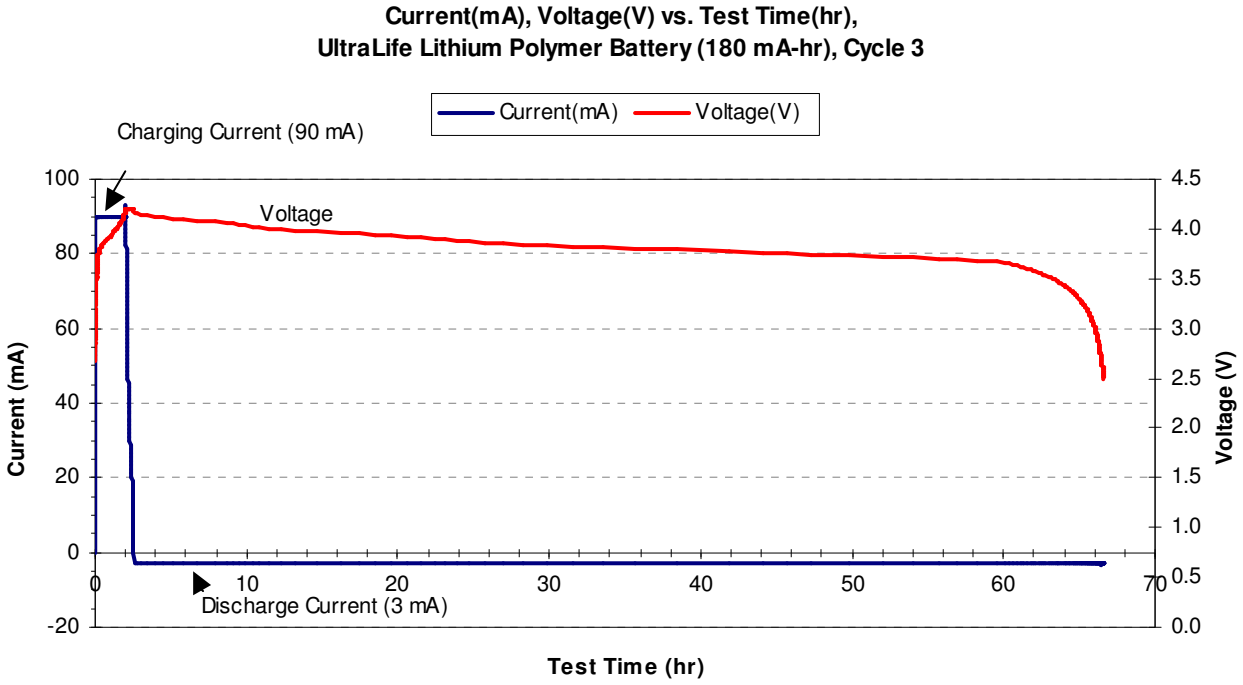

Figure 5. A cycled battery charge/discharge curve for the lithium polymer battery.

The results of the cycled charge/discharge test are shown in Figure 5. For this test, the battery tester was programmed to charge the battery to 4.2 volts at a charging current of 90 mA. It then switched to discharging the battery at a constant 3 mA current. The test was programmed to end when the battery voltage decreased to 2.5 volts. With these parameters, the battery lasted

for 66.7 hours, for a measured capacity of 200 mA·hrs. Both methods indicated that the battery capacity would be higher than the manufacturer's 180 mA·hr rated capacity. Thus, even if the module was used 16 hours a day, it would be able to last four days before it would need to be recharged. It is anticipated that neuroprosthesis users will recharge their systems either nightly or ever other night.

Next Quarter

In the next quarter, we will work with a manufacturer who has been selected to miniaturize the design of the WDAM. Several prototypes will be manufactured, and a custom enclosure will be designed. Also in the next quarter, we will investigate optimizing the data packet parameters and filter settings for the "medium-speed" and "high-speed" WDAM versions.

References

[1] Z. Matjacic, M. Munih, T. Bajd, A. Kralj, H. Benko, and P. Obreza, "Wireless control of functional electrical stimulation systems," *Artif Organs*, vol. 21, pp. 197-200, 1997.

Neural Network Controller for an Upper Extremity Neuroprosthesis

Contract section: E.2.a.ii.4.1 EMG-based shoulder and elbow controller

Abstract

The long term goal of this project is to develop a controller for an upper extremity neuroprosthesis targeted for people with C5/C6 spinal cord injury (SCI). The challenge is to determine how to simultaneously stimulate different paralyzed muscles based on the EMG activity of muscles under retained voluntary control. The proposed controller extracts information from the recorded EMG signals and processes this information to generate the appropriate stimulation levels to activate the paralyzed muscles. The goal of this project was to design and evaluate this controller using a dynamic, three-dimensional musculoskeletal model of the arm. Different arm movements were recorded from able bodied subjects and these kinematics served as input to the model. The model was modified to reflect C5/C6 SCI, and inverse simulations were run to provide muscle activation patterns corresponding to the movements recorded. A set of "voluntary" and "paralyzed" muscles was selected for the controller based on each muscle's relevance as suggested by the simulations. Activation patterns were then used to train a dynamic neural network that predicts "paralyzed" muscle activations from "voluntary" muscle activations. The neural network controller was able to predict the activation level of three paralyzed muscles with less than 2% average prediction error, using four input muscles as inputs.

Introduction

Individuals with C5/C6 SCI lose control over a number of muscles in their upper extremity. Their hand muscles are paralyzed, there is partial loss of wrist and elbow extension, and several shoulder functions are lost, including horizontal flexion and adduction. Arm movements are a coordinated action of several muscles acting upon different joints resulting in a large workspace and fine positioning control. Paralysis of some these muscles lead to a considerable reduction in the reachable workspace. Functional Electrical Stimulation (FES) can

be used to stimulate paralyzed muscles whose innervations remain intact, restoring function in individuals with SCI. However, determining the timing and intensity required for simultaneously stimulating different paralyzed muscles in the arm is still a big challenge.

The long term goal of this project is to determine which, how and when to stimulate each of the available muscles in a coordinated fashion to increase the arm's workspace and thus provide a functional benefit to the paralyzed individual. The proposed approach exploits retained voluntary function by extracting the movement intention from the EMG activity of muscles that are under voluntary control and using this information to determine the levels of stimulation required. Based on this principle, positioning and stability in the limb become a synergistic action between the remaining nervous system and the adaptive mechanism of the artificial controller.

Previous work in our lab has shown that an approach of this kind is feasible. Au et al. [1] demonstrated that a neural network is capable of predicting shoulder and elbow joint angles using EMG signals from selected muscles. Parikh et al. [2] used a musculoskeletal model of the arm to obtain the muscle activations required to hold the arm in a certain posture and then used a neural network to predict paralyzed muscle activations using voluntary muscle activations as inputs. Finally, Giuffrida [3] used a neural network to predict triceps stimulation levels for elbow extension using the EMG activity from four arm muscles as the input. This work gives strong evidence that EMG signals are useful to predict movement intention and generate adequate stimulation patterns.

The specific goal of this study was to show the feasibility of controlling a neuroprosthesis using retained voluntary function by designing a neural network-based controller that will estimate the activation levels of paralyzed muscles using the activation levels of voluntary controlled muscles as inputs. In a future application the controller will determine the stimulation levels for a neuroprosthesis that will restore multiple arm functions simultaneously.

Methods

A. General Approach

Figure 6 summarizes the overall approach used in this study. Experiments were conducted during which the kinematics of the upper extremity of able-bodied subjects were recorded during a series of arm movements. These data were processed to obtain the kinematics of the shoulder and elbow joints. The kinematics became the input to a musculoskeletal model of the shoulder and elbow that was modified to reflect a C5 SCI individual by reducing the maximal

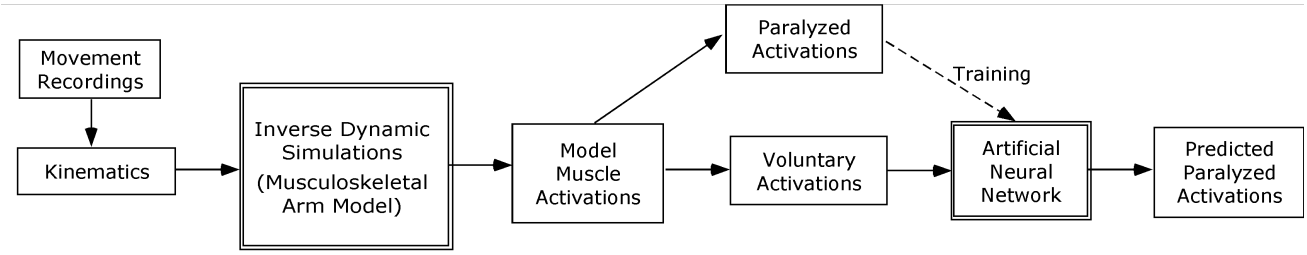

Figure 6. Approach to develop the controller.

forces that each muscle could generate, including setting muscles that are typically paralyzed to have zero maximum force. Furthermore, the maximum force of three paralyzed muscles was set to 50% of able-bodied maximum activation to simulate the potential of FES to generate force in those muscles. Inverse dynamic simulations were run to predict the muscle activation patterns, both "voluntary" and "paralyzed", necessary to drive the movements recorded. An artificial neural network was then trained to predict 'paralyzed' muscle activations from 'voluntary' muscle activations, mimicking the real situation where EMG signals from voluntarily controlled muscles will be processed by a neuroprosthesis controller and used to determine the appropriate levels of stimulation for paralyzed muscles.

B. Experimental Recordings.

Arm movements from able-bodied subjects were recorded using an Optotrak motion analysis system (Northern Digital Inc.) as shown in Figure 7. Sets of LED clusters were fixed over the thorax, upper arm and forearm of the subject. The locations of the scapula and clavicle were difficult to track dynamically so a scapular palpator with a fourth cluster of LEDs was used to track the position of the scapula during static trials in different positions within the workspace [4]. This data and the dynamical orientation of the humerus were used to recover the orientation of the scapula and the clavicle representing a standard shoulder rhythm [5]. Specific bony landmarks were recovered during the movements in order to generate coordinate systems and obtain orientations for each joint in the shoulder and elbow. The recording and data processing were done following the International Shoulder Group recommendations for shoulder and elbow recordings [6, 7]. The movements performed included both single joint movements (shoulder abduction/adduction, flexion/ extension, horizontal flexion/extension, internal/external rotation and elbow flexion/extension and pronation/supination) and a set of functional movements comprised of activities of daily living (ADL) such as feeding and reaching objects. Data were recorded at 50Hz.

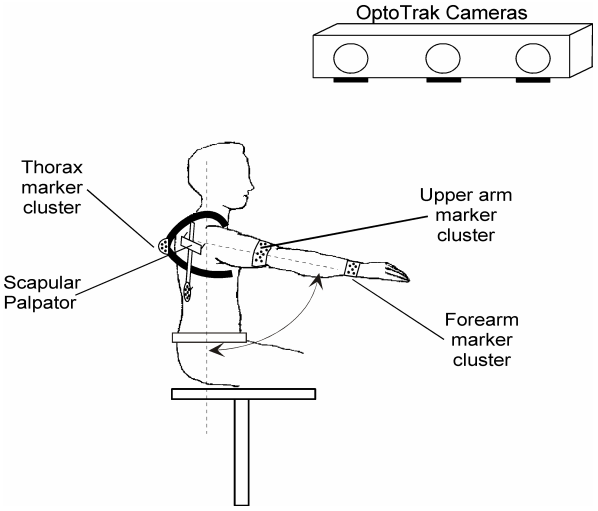

Figure 7. Experimental Setup

C. Simulations with Musculoskeletal Model

Inverse dynamic simulations were run with a musculoskeletal model of the shoulder and elbow to estimate muscle activation patterns needed for an SCI-modified muscle set to generate the recorded movements. The model was developed at the Delft University of Technology [8] and consisted of the five bones of the arm (thorax, clavicle, and scapula, humerus, radius and ulna), 29 muscles, the conoid ligament and 17 degrees of freedom distributed over five joints. The model was modified to reflect the conditions of a C5/C6 SCI subject by decreasing the maximum forces that could be generated by each muscle. Muscles with some voluntary control have nonzero maximum activations, while paralyzed muscles have zero maximum activation.

Several paralyzed muscles that could be stimulated to produce muscle contractions were included in some simulations with a maximum activation of 0.5.

D. Muscle Selection

To select a set of 'paralyzed' muscles for electrical stimulation, extensive simulations were done with the 'voluntary' muscles augmented with different combinations of 'stimulated' muscles. A realistic selection consistent with a future application requires a set of 'stimulated' muscles that is paralyzed but not denervated in a typical C5 SCI individual, and also they must be important contributors to the movements and functional tasks to be restored. This was evaluated using the outcomes of the simulations performed with the model, and the muscles were chosen based on the need for their mechanical contributions. First, simulations were performed with an able-bodied model (i.e. no force reductions). The estimated maximum activations for the tested movements were compared with those available in the reduced C5 SCI model (without any added "stimulated" muscles). Muscles that required more activation than could be provided by the C5 model were selected for possible inclusion in the 'stimulated' muscle set. Second, the percentage of failure of simulations that included the "stimulated" muscle set was used to determine the minimal set of muscles required to successfully perform the movements recorded during the experiments.

To select a set of 'voluntary' muscles to extract information and become input to the controller, they should be under at least partial voluntary control and be available for EMG recordings in a neuroprosthesis. A multi-input multi-output (MIMO) system identification technique was used with able-bodied data to obtain the frequency response between 12 input "voluntary" muscle activations, and the activation of the three muscles ultimately chosen as output "stimulated" muscles. The partial coherences between each potential input muscle and the three output muscles was used to assess common information that would indicate which input muscles were likely to be the most effective in predicting needed output activations

E. Artificial Neural Network

The goal of the eventual FES controller is to predict the stimulation levels needed in paralyzed muscles using information from activations of muscles under voluntary control. We evaluated the use of an artificial neural network (ANN) to map the dynamic and nonlinear relationship between the input and output muscle activations. A typical two layer feed-forward ANN with a non-linear tangent-sigmoidal activation function for the hidden layer and a linear output layer was used. The performance of all the trained networks was measured as the ability to predict data not used during the training, i.e. the ability to generalize. This is a highly desirable feature of the controller because it must be capable of assisting movements in many different conditions and locations, not just in the specific ones used during training. The data was split into training, validation and testing data sets. Validation is used during the training to monitor the error generated by data not used for training. When this error increases, the ANN is memorizing the training data set and the network is loosing its ability to generalize. The testing data set is used to evaluate the performance of the ANN after the training is finished. The goodness of fit of the ANN was quantified as the average RMS error between the original model-generated muscle activations (for the "stimulated" muscles) and those predicted by the ANN based on "voluntary" muscle activations. All prediction errors in the Results will be presented as a percentage of

maximum muscle activation. All ANNs were trained using MATLAB's Neural Network Toolbox (The Math Works, Inc.).

Results

A. Musculoskeletal Model: Kinematic Input And Muscle Activation Output

Figure 8 shows an example of a typical input and output data trial corresponding to fifteen seconds of reaching movements at the shoulder level. The top five plots show the Euler angles describing the orientation of the thorax, clavicle, scapula, humerus and forearm. Each plot shows lines corresponding to each joint's degrees of freedom (three in the shoulder joints and two in the elbow). The lower six plots show the model-predicted activation patterns of six representative muscles during this movement. They are the output of a simulation corresponding to a C5 SCI individual with FES of the three paralyzed muscles selected as will be shown below.

B. Muscle Selection

Three paralyzed muscles including serratus anterior, triceps, and pectoralis major were found to be the most critical for adding back into the model as 'stimulated' muscles. By removing muscles one at a time from the 'stimulated' muscle set, it was clear that the serratus anterior was critical for all the movements – the failure rate was very close to 100%. When triceps was not present in the stimulation set, mean failure was 8% and it was a key muscle for the ADL task of eating (19.8%) and for high reach movements (44.3%). The pectoralis major (clavicular portion) was chosen for its contribution during high reaching movements and horizontal flexion movements towards the center of the workspace (46.3% and 11.5% failure respectively).

Four voluntary controlled input muscles including trapezius, deltoid, supraspinatus and supinator were selected for having higher partial coherences resulting from the MIMO system identification procedure performed between the 12 candidate input muscles and the three 'stimulated' output muscles. Variations over this set that included

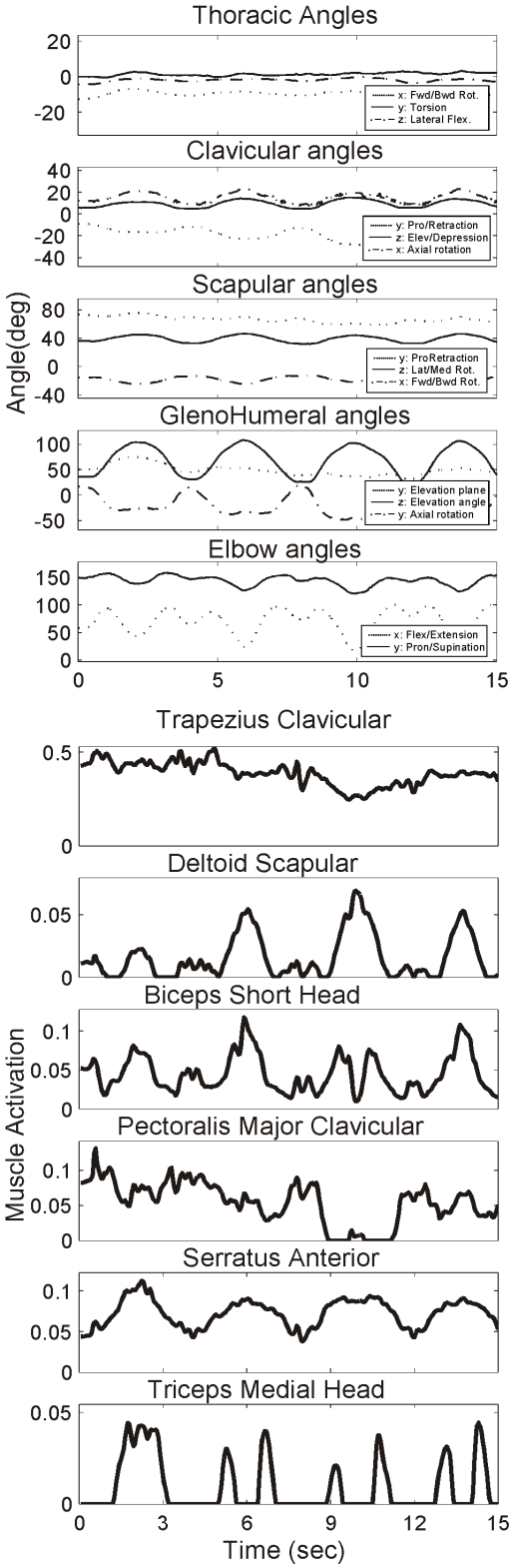

Figure 8. Model input and output.

the Biceps and Brachioradialis were also tried, obtaining similar prediction results. This demonstrated that four muscles is a feasible quantity for a real application and that there is probably a broad range of muscles to choose from in the C5/C6 SCI population.

C. Neural Network Predictions.

Figure 9 is an example of a 15 second trial representing a reaching movement above the shoulder level. The first plot shows humerus elevation and elbow flexion/extension angles illustrating the movement performed. The second plot shows the "voluntary" activations used as inputs in this particular case to predict the "paralyzed" muscle activations. The lower plots show the prediction of each output paralyzed muscle. Solid lines show the neural network predictions and dotted lines show the target muscle activations generated by the model. The mean prediction error for these three muscles during this particular movement was 1.44% of maximum muscle activation. Notice that the prediction has the same dynamic characteristics of the simulated activations and that the muscle activations are predicted quite accurately.

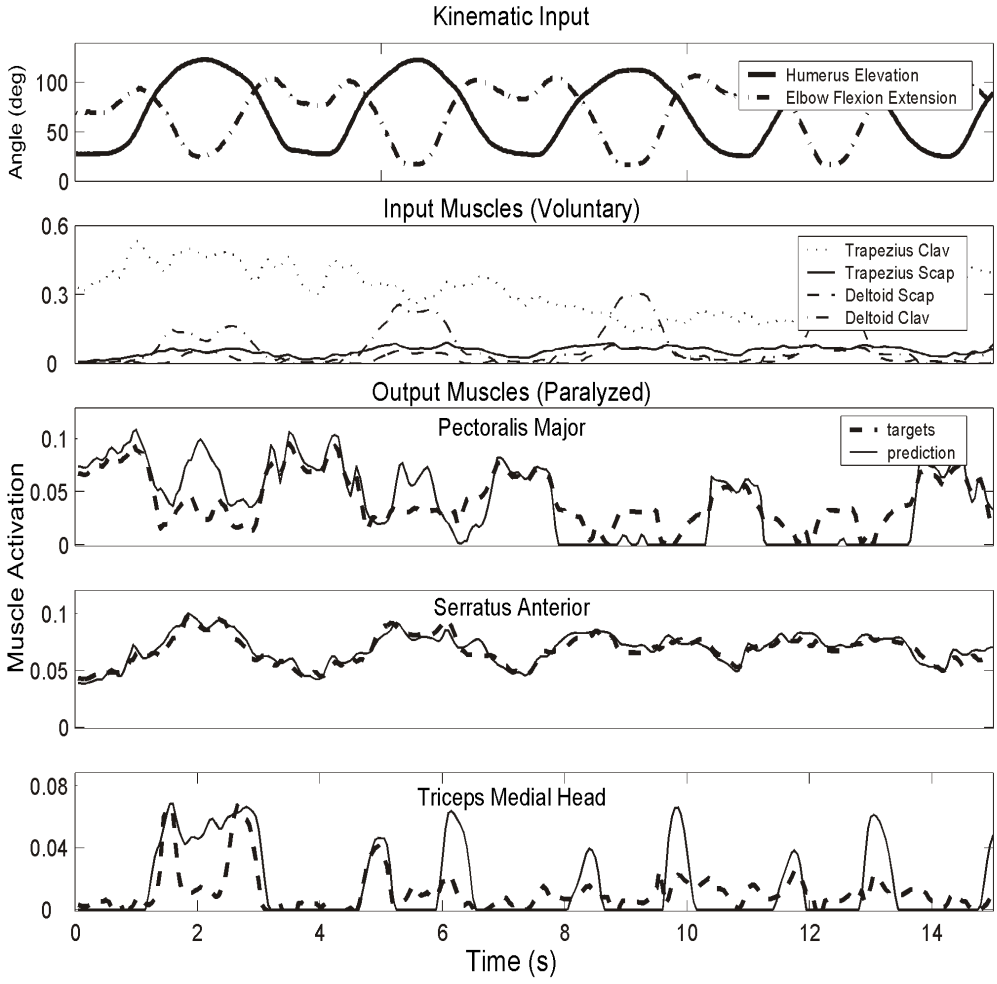

Figure 9. Reaching above the shoulder level trial (15 sec). Solid lines show the prediction and dashed lines show the target activations generated by the model.

Discussion

The goal of this study was the design of a controller capable of using retained voluntary function to extract the movement intention and generate the appropriate levels of stimulation for paralyzed muscles in people with C5/C6 SCI. After recording movements during experiments with able-bodied subjects and obtaining muscle activation patterns from inverse dynamic simulations with a musculoskeletal model of the arm, an artificial neural network was successfully trained to predict paralyzed muscle activations using voluntary muscle activations as inputs.

These preliminary findings demonstrated that an ANN is a good open-loop block for the proposed controller. It was capable of predicting muscle activations with an accuracy of less than 2%. EMG signals are representative of muscle activations levels; therefore, this approach can be implemented in humans by using signals directly recorded from voluntarily controlled muscles. Errors are anticipated using an open loop strategy as it does not account for changes in the arm properties during different activities and conditions (e.g. fatigue). If the user is not able to compensate voluntarily for these expected errors, an adaptive element that accounts for these disturbances can be added as a feedback block for the controller.

Incorporating retained voluntary control mechanisms exploits the immense adaptive ability of the human nervous system. The hypothesis of this work is that intact portions of the nervous system can readapt to the use of the neuroprosthesis and learn to interact with it. The proposed controller will successfully interact with the remaining motor function in a continuous adaptation process creating a synergistic relation between the nervous system and the neuroprosthesis that will restore function in a natural manner.

References

[1] Au A., Kirsch R.F. "EMG-Based prediction of shoulder and elbow kinematics in able-bodied and spinal cord injured individuals". IEEE Transactions on Rehabilitation Engineering. Vol 8, No 4. Dec 2000.

[2] Parikh P.P. "Voluntary synergistic control of shoulder muscle functional neuromuscular stimulation patterns in C5 tetraplegia". MSc. Thesis. Biomedical Engineering. Case Western Reserve University. 1999.

[3] Guiffrida J.P, "Synergistic neural network control of FES elbow extension after SCI using EMG". Ph.D. Thesis. Biomedical Engineering. Case Western Reserve University. 2004.

[4] Veeger,H.E.J., van der Helm, F.C.T., Chadwick, E.KJ., Magermans, D. "Toward standardized procedures for recording and describing 3-D shoulder movements". Behavior Research Methods Instruments & Computers. 35 (3). Pp 440-446. 2003.

[5] De Groot, J.H., Brand, R. "A three-dimensional regression model of the shoulder rhythm" Clinical Biomechanics. Vol. 16 (2001) 735-743.

[6] Van der Helm F.C.T. "A standardized protocol for motion recordings of the shoulder". Proceedings of the First Conference of the International Shoulder Group. 1997.

[7] Van der Helm, F.C.T. et al. "ISB recommendation on definitions of joint co-ordinate system of various joints for the reporting of human motion: Pt II. Shoulder and Elbow. Journal of Biomechanics. In press.

[8] Van der Helm, F.C.T. "A finite element musculoskeletal model of the shoulder mechanism". Journal of Biomechanics. Vol 27. No 5. pp 551-569. 1994.

Feed-Forward Control of Neuroprosthetic Systems Characterized by Redundant Muscles Acting on Multiple Degrees of Freedom

Contract section:

E.2.a.ii. Simultaneous and natural control of multiple arm and hand functions.

Abstract

We created a time-varying static biomechanical model of the thumb that will allow us to generate time-varying, coupled, and redundant input-output data (i.e., isometric forces at the tip of the thumb in response to electrical stimuli).

Objectives

We previously developed a method for implementing feedforward neuroprosthetic controllers for musculoskeletal systems with multiple degrees of freedom and complex mechanical interactions. These controllers rely on inverse models of the musculoskeletal systems under control. Our tests showed that controller performance was poorer than we expected, and we attribute the poor performance to redundancy of the data used to train the controllers. The inverse relationship between muscle output and electrical stimulation is not unique (most joints have redundant actuation with non-stationary input-output muscle properties and coupled degrees of freedom) and if left unrestricted, the controller implementation process may result in an unsuitable inverse. Thus, we must choose a single inverse solution before the controller can be created. Our present work involves obtaining this unique inverse solution and using it to train a controller capable of providing independent control of coupled degrees of freedom.

Our general approach will be to first create a time-invariant forward neural network model of the thumb using time-varying, coupled and redundant data relating muscle stimuli to muscle outputs. We will use the forward model to average the input-output data and thus eliminate its time-variance. We will then choose unique input-output data from the time-invariant set that optimize specific performance criteria, such as minimum co-activation, allowing us to eliminate redundancy, obtaining thus a unique solution. We will train an inverse-model, static, feedforward, artificial neural network controller with these optimal input-output data. We will create, in simulation, a time-varying static biomechanical forward model of the thumb, which we will use as a test-bed prior to experimental studies to generate time-varying, coupled and redundant input-output data. We will test the controller isometrically with the simulation model and with able-bodied and spinal cord injured human subjects. We will first study redundancy by stimulating only a pair of antagonists (extensor pollicis longus and abductor pollicis brevis) controlling flexion/extension of the thumb's carpometacarpal joint. We will incorporate coupling to the system by stimulating two additional muscles (flexor pollicis longus and adductor pollicis) allowing us to control abduction/adduction as well. We will use the same approach for all computer model and real musculoskeletal systems studies.

Structure of the biomechanical model

A time-varying static biomechanical model of the thumb was created that allows us to generate input-output data that are time-varying, coupled, and redundant (i.e., isometric forces at the tip of the thumb in response to electrical stimuli). We modeled the metacarpal bone and phalanges with cylindrical rigid bodies (Table 3) joined by two joints. The skeletal model parameters were taken from the literature [Valero-Cuevas et al. 2003, Secco Magenes 2002,

Lewis 2001]. We fixed the interphalangeal (IP) joint and modeled the proximal and distal phalanges as a single rigid body (Figure 10). We modeled the metacarpophalangeal (MP) joint as a revolute joint linking the metacarpal to the phalanges, and the carpometacarpal (CMC) joint as a universal joint linking the metacarpal bone to the trapezium, which will be fixed in space (i.e., no arm rotation will be allowed). The tip of the thumb was also fixed in space to a force/moment sensor so we could measure isometric forces.

Table 3. Skeletal parameters of the thumb.

Bone	Length (cm)	Radius (cm)	Specific mass (g/cm^3)
Metacarpal	7.20	1.50	1.1
Proximal phalanx	3.90	1.10	1.1
Distal phalanx	2.00	1.10	1.1

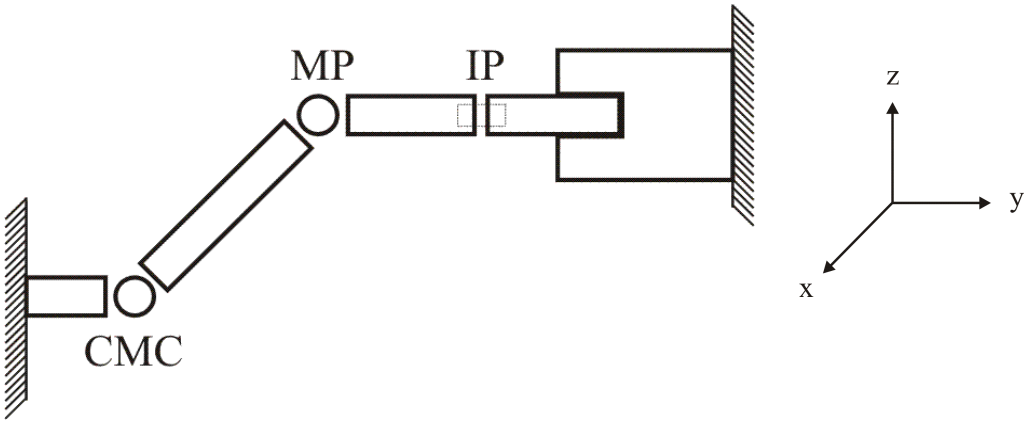

Figure 10. The trapezium and the tip of the thumb are both fixed in space. The IP joint is fixed. The MP joint is modeled as a revolute joint while the CMC joint is modeled as a universal joint.

We control the isometric forces at the tip of the thumb through forces and moments acting upon the CMC and MP joints. Its coupled degrees of freedom (i.e., flexion/extension and abduction/adduction) actuated by redundant muscles can be excited in human subjects with the use of an implanted upper-extremity neuroprosthesis or surface stimulation.

The peak isometric force and muscle geometric parameters for four muscles included in the model (extensor pollicis longus (EPL), flexor pollicis longus (FPL), abductor pollicis brevis (AbPB), and adductor pollicis (AdP)) were taken from the literature [Esteki and Mansour 1997, Jacobson et al. 1992, Lieber et al. 1992, Brand et al. 1981] and are summarized in Table 4.

Table 4. Muscle parameters. Lo represents the optimal muscle length. Fo is the maximum force produced when the muscle is at its optimal length. Lst is the tendon slack length.

Muscle	Lo (cm)	Fo (N)	Lst (cm)
EPL	5.7	38	21
FPL	5.9	102	32.15
AdPo	3.6	18	2.25
AdPt	3.6	48	3.5
AbPB	3.7	30	2.55

Individual muscle forces (F_m) depend primarily upon their muscle activations and time. We used a Hill based muscle model incorporating length-tension properties. We omitted activation dynamics and force-velocity properties because we will perform static analysis only.

$$\tilde{F}_m = f(i)AF_o\left[L\tilde{T}\left(\tilde{L}_m\right)\right]$$

$$L\tilde{T}\left(\tilde{L}_m\right) = -3.05\tilde{L}_m^{\ 2} + 5.98\tilde{L}_m - 1.96$$

$$\tilde{L}_m = L_m / L_o$$

$$L_m = L_{mt} - L_t$$

$$L_{mt} = L' + \int_0^{\theta_2} r(\theta_2)d\theta_2 + \int_0^{\theta_1} r(\theta_1)d\theta_1 + \int_0^{\phi_1} r(\phi_1)d\phi_1$$

$$L_t = L_{st} + F_m / K_T$$

$$K_T = \frac{F_o}{0.0325L_{st}}$$

where

F_m = muscle force
f(i) = fatigue factor
A = muscle activation
K_T = tendon stiffness
r = moment arm
θ_2 = MP flexion/extension angle
θ_1 = CMC flexion/extension angle
ϕ_1 = CMC abduction/adduction angle
L_m = muscle length
L_t = tendon length
L_{mt} = muscle-tendon length
L_{st} = tendon slack length
L' = muscle-tendon unit length when all joints are at 0^o
L_o = optimal muscle fiber length
~ = normalized

Muscle activation is modeled as a nonlinear function of the electrical stimulus given by a

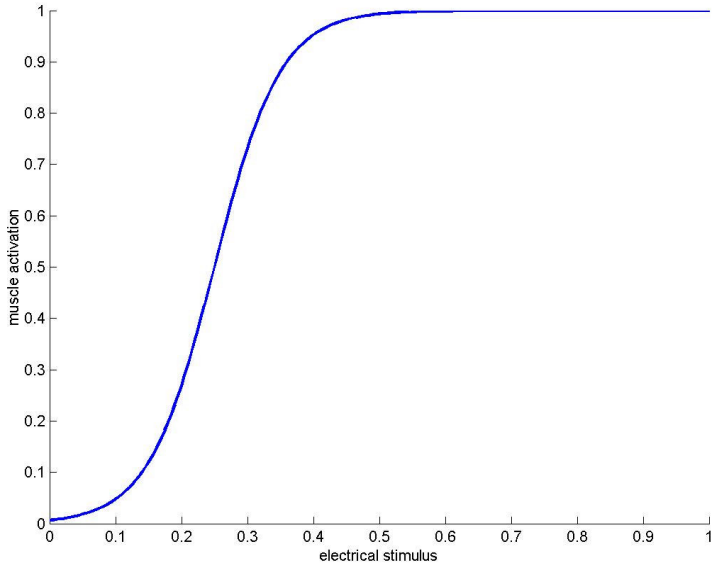

Figure 11. Simple nonlinear recruitment characteristics. Muscle activation as a function of normalized muscle stimulus.

sigmoidal relationship of the form $A(u) = \frac{1}{\left(1+e^{-u}\right)}$ (Figure 11).

To account for the time-varying properties of muscle, we introduce the linearly-decreasing normalized fatigue factor *f(i)* (Figure 12) to scale the maximum muscle force $\widehat{F}_o$. The fatigue factor reduces the maximum muscle force by 0.042% with every muscle contraction. This rate is based on a 15% reduction after approximately 360 contractions in recruitment tests performed by Kilgore [Kilgore 1987]. We also add or subtract random noise (as a percentage of the maximum muscle force) to the muscle force (F_m) with every muscle contraction. We assume muscle potentiation is eliminated by conditioning contractions prior to performing any measurements.

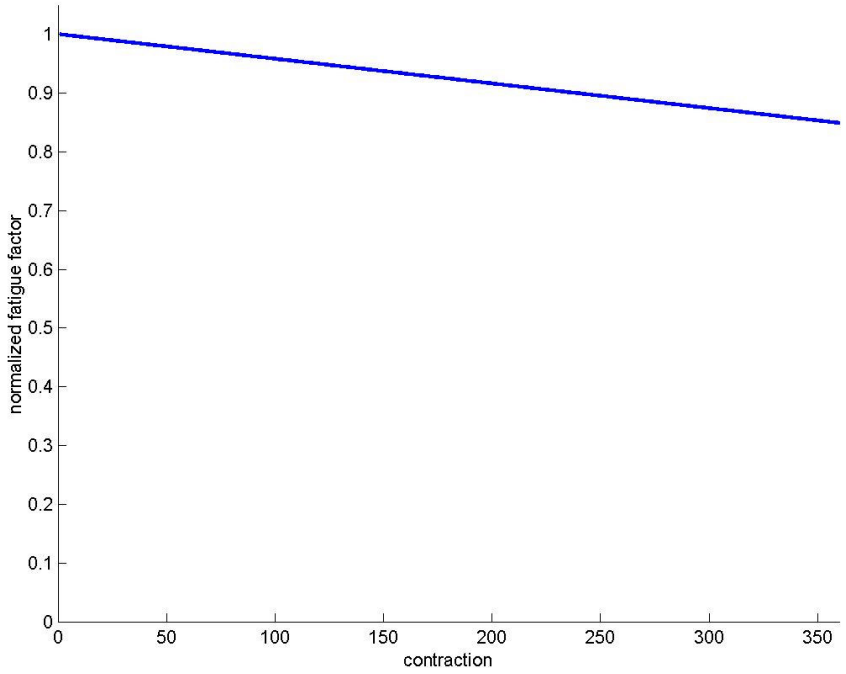

Figure 12. Normalized fatigue factor *f(i)* as a function of muscle contraction.

The thumb joints are acted upon by active and external forces/moments, due to muscle contraction, gravitation, and contact forces (Figure 13). In our application, we control the muscle forces by stimulation, and measure the contact forces/moments at the thumb tip. Thus, we will write six equations balancing the moments and forces in all three directions, and solve for the six contact forces/moments.

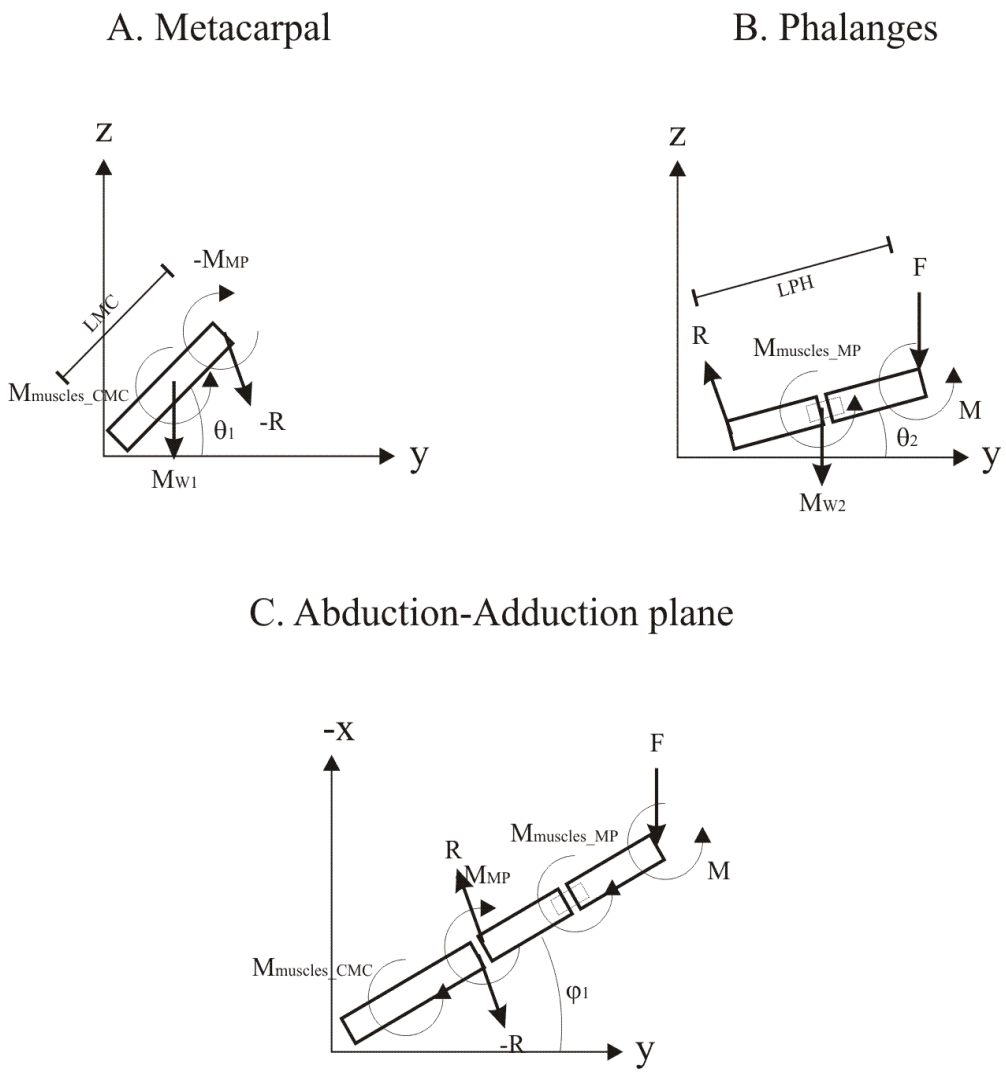

Figure 13. Free body diagrams of the metacarpal and phalangeal links. Both links have the same orientation in space with respect to the abduction/adduction plane, given by ϕ_1.

The moments at the MP joint are those due to the contact force (M_F), the weight of the phalanges (M_{W2}), the contact moment (M), and the muscles crossing the MP joint ($M_{muscles\_MP}$). The sum of the forces at the MP joint must also be zero.

$$M_{MP(j)} = 0 = M_{F(j)} + M_{W2(j)} + M_{(j)} + M_{muscles\_MP(j)}$$

$0 = R_{(j)} + F_{(j)} + F_{W2(j)}$. Therefore, the reaction force is $R_{(j)} = -\left(F_{(j)} + F_{W2(j)}\right)$; *for* $j = x,y,z$

At the CMC joint, the moments are those due to the reaction force at the MP joint (M_R), the weights of the metacarpal (M_{WI}), the moment at the MP joint (M_{MP}), and the muscles crossing the CMC joint ($M_{muscles\_CMC}$).

$$M_{CMC(j)} = 0 = M_{WI(j)} + M_{muscles\_CMC(j)} + M_{R(j)} + M_{MP(j)} \qquad ; for\ j = x,y,z$$

We do not include the equations for the joint contact force at the CMC joint because we do not need to know this force.

The individual moments are given by the following equations. The muscle moment equations are given in the global coordinate system, assuming ϕ is zero.

$$M_{muscles\_MPx} = \sum_{i=1}^{n} r_i(\theta_2) \times F_{m\_i} \qquad M_{muscles\_CMCx} = \sum_{i=1}^{n} r_i(\theta_1) \times F_{m\_i}$$

$$M_{muscles\_MPy} = 0 \qquad M_{muscles\_CMCy} = 0$$

$$M_{muscles\_MPz} = 0 \qquad M_{muscles\_CMCz} = \sum_{i=1}^{n} r_i(\phi_1) \times F_{m\_i}$$

$$M_{W2x} = LPH/2 \cos(\theta_2)(m_2 g) \qquad M_{W1x} = LMC/2 \cos(\theta_1)(m_1 g)$$

$$M_{W2y} = -LPH/2 \sin(\phi_1)(m_2 g) \qquad M_{W1y} = -LMC/2 \sin(\phi_1)(m_1 g)$$

$$M_{W2z} = 0 \qquad M_{W1z} = 0$$

$$M_{Fx} = LPH \cos(\theta_2) F_z - LPH \sin(\theta_2) F_y$$
$$M_{Fy} = LPH \sin(\theta_2) F_x - LPH \sin(\phi_1) F_z$$
$$M_{Fz} = LPH \sin(\phi_1) F_y - LPH \cos(\theta_2) F_x$$

$$M_{Rx} = -LMC \cos(\theta_1) R_z + LMC \sin(\theta_1) R_y$$
$$M_{Ry} = -LMC \sin(\theta_1) R_x + LMC \sin(\phi_1) R_z$$
$$M_{Rz} = -LMC \sin(\phi_1) R_y + LMC \cos(\theta_1) R_x$$

where,

F	=	Force exerted at the tip of the thumb.	M	=	Contact moment exerted at the tip of the thumb.
R	=	Resultant force at the MP joint.	M_F	=	Moment due to the thumb tip force at the MP joint.
W_1	=	Weight of the carpal bone (link 1).	M_R	=	Moment at the CMC joint due to the resultant force applied at the MP joint.
W_2	=	Weight of the phalanges (second link).	M_{W1}	=	Moment exerted on the CMC joint due to the weight of the carpal bone.
LPH	=	Phalangeal length.	M_{W2}	=	Moment exerted on the MP joint due to the weight of the phalanges.
LMC	=	Metacarpal length.	$M_{Muscles\_MP}$	=	Muscle moment exerted at the MP joint.
n	=	Number of muscles.	$M_{Muscles\_CMC}$	=	Muscle moment exerted at the CMC joint.

m_1 = Metacarpal mass.

m_2 = Phalangeal mass.

g = Gravitational constant.

Next Quarter

Next quarter we will complete and validate the implementation of the model. We will generate time-varying coupled and redundant input-output data. We will create a time-invariant forward neural network model of the thumb from these data, and use this forward model to average the input-output data and thus eliminate its time-variance. We will also optimize the averaged input-output data using a minimum co-activation criterion to eliminate redundancy and coupling, obtaining thus a unique solution. Finally, we will use the optimized input-output data to train a static feedforward artificial neural network controller. We will test this inverse-model feedforward controller isometrically in simulation with the biomechanical model of the thumb.

References

Brand P.W., Beach R.B., Thompson D.E. (1981) "Relative tension and potential excursion of muscles in the forearm and hand", *J. Hand Surgery [Am]*, Vol. 6 (3), May, 209-219.

Esteki A., Mansour J.M. (1997) "A dynamic model of the hand with application in functional neuromuscular stimulation", *Annals of Biomedical Engineering*, Vol. 25, No 5.

Jacobson M.D., Raab R., Fazeli B.M., Abrams R.A., Botte M.J., Lieber R.L. (1992) "Architectural design of the human intrinsic hand muscles", *J. Hand Surgery [Am]*, Vol. 17A (5), Sept, 804-809.

Kilgore K.L. (1987) "Force vector recruitment of electrically stimulated paralyzed thenar muscles with application to functional neuromuscular stimulation", M.S. Thesis, Case Western Reserve University.

Lewis S. (2001) "Metacarpophalangeal pattern profile analysis of a sample drawn from a North Wales population", *Annals of Human Biology,* Vol. 28 (5), 589-593.

Lieber R.L., Jacobson M.D., Fazeli B.M., Abrams R.A., Botte M.J. (1992) "Architecture of selected muscles of arm and forearm: anatomy and implications for tendon transfer.", *J. Hand Surgery [Am]*, Vol. 17A (5), Sept, 787-799.

Secco E.L., Magenes G. (2002) "A life-like control algorithm for the natural movement of a 3 DOF finger", *Proceedings of the Second Joint EMBS/BMES Conference*, Houston, TX. USA. October 23-26.

Valero-Cuevas F.J., Johanson M.E., Towles J.D. (2003) "Towards a realistic biomechanical model of the thumb: the choice of kinematic description may be more critical than the solution

method or the variability/uncertainty of musculoskeletal parameters", *Journal of Biomechanics,* Vol. 36, 1019–1030

An Implanted Neuroprosthesis For Electrical Stimulation through Nerve- and Muscle-based Electrodes and Myoelectric Recording

Contract section:
E.1.a.vi Implementation and evaluation of neuroprostheses for high tetraplegia

Introduction

The goal of this section of the project is to develop the hardware components necessary to implement advanced neuroprostheses for high tetraplegia. The key component of this effort is the development of an implanted stimulator/telemeter device that is capable of both electrical stimulation and myoelectric recording. Specifically, we are designing and fabricating an implanted neuroprosthesis that is capable of 12 channels of stimulation and has two channels of myoelectric signal (MES) recording, referred to as the implantable stimulator-telemeter-12 (IST-12). The myoelectric signal recording has been successfully demonstrated in-vivo, and is now being implemented with human subjects (in a separate project). With this phase of development completed, we are now addressing the specific stimulation capabilities of this device that are needed for this contract. Specifically, the device must be capable of safely and effectively delivering stimulus parameters that are appropriate for stimulation using muscle-based electrodes **and** nerve-based electrodes.

Design Modifications

The stimulus output stage of the IST utilizes capacitive coupling to activate the muscle tissue via the muscle-based electrodes. In this capacitively-coupled design, a finite amount of inadvertent anodic current, 0.5 milliamps or less, occurs on unstimulated channels during the cathodic phase of the stimulated channel. This poses no problem if all the implanted electrodes in the system are muscle-based since the current threshold for muscles is well above 0.5 milliamps. In our systems, the current used to activate muscle tissue is normally 20 mA, at least 40 times this inadvertent anodic current. Mixed-electrode type (i.e. muscle and nerve electrodes) systems like those proposed in this study may pose a problem since the stimulus threshold for nerves is at much lower currents than for muscles. Our inadvertent anodic current "leakage" is of sufficient amplitude to activate neural structures in direct contact with nerve cuff electrodes. To address this issue and eliminate the inadvertent activation of nerves during stimulation of muscle-based electrodes, we have taken the following measures: 1) we modified the design of the circuit to create an open–circuit that interrupts the current path to all other electrodes when any one electrode from that same device is stimulating. 2) we employed a design feature that enables implants to be coded with one of four unique ID codes enabling RF identification of each stimulating device and addressing each device uniquely. Additionally, each implant will recognize stimulus commands that are being addressed to other implants. This will enable activation of one stimulator while the others are instructed to remain 'quiet' (no stimulation).

We have bench-tested both circuit modifications with success, and have integrated them into the circuit-board design and fabrication. We are confident that these circuit modifications, coupled with spatial separation of the devices within the body, will eliminate the possibility of

inadvertent activation of neural structures enclosed within the implanted cuff electrodes while muscle-based electrodes are being stimulated.